Supplementary Material for Srivastava, Sengupta, and Ghosh (2024), "Quantifying the rhythm of ice accumulation in East Antarctica with varying temperature": Variations of the model

1. A model for nonlinear effect of temperature

An extension of the model (1) of the main paper, which allows a nonlinear effect of temperature on AAR is:

$$b_i = \left(1 + \gamma_1 x_i + \gamma_2 x_i^2\right) g(z_i)\xi_i \text{ for } i = 1,2, \dots, n, \quad \text{(S.1)}$$

where γ_1 and γ_2 are unspecified parameters, g is an unspecified decreasing function, and the factor ξ_i is a multiplicative random error. The parameters γ_1 and γ_2 and the function g can be estimated from the data in the manner described in the last paragraph of Section 2 of the main paper.

1.2 Results

The model (S.1) is fitted to the three data sets separately for the age segments 0 to 125 kyr, 125 to 410 kyr and 410 to 800 kyr. Table S.1 gives the estimated values of γ_1 and γ_2 along with the bootstrap standard error (with 95% confidence interval) for the different parts of the three data sets.

Table S.1: Estimates of the parameters $\gamma_1$and γ_2 model (Quad) along with standard error and 95% CI

Site	Attribute	Estimated γ (per ^{0}C), standard error and 95% CI		
		Ages prior to 125 kyr	Ages between 125 to 410 kyr	Ages after 410 kyr
Dome Fuji	Estimated γ_1 Estimated γ_2	0.0418 -0.0019	0.1267 0.0124	0.0892 0.0048
	Estimated se γ_1 Estimated se γ_2	0.0160 0.0029	0.0101 0.0021	0.0367 0.0068
	95% CI γ_1 95% CI γ_2	(0.0168, 0.0813) (-0.0078, 0.0037)	(0.1063, 0.1462) (0.0083, 0.0165)	(0.0072, 0.1470) (-0.0104, 0.0164)
Lake Vostok	Estimated γ_1 Estimated γ_2	0.0532 -0.0007	0.0690 0.0015	
	Estimated se γ_1 Estimated se γ_2	0.0367 0.0041	0.0063 0.0007	
	95% CI γ_1 95% CI γ_2	(-0.0353, 0.1089) (-0.0107, 0.0056)	(0.0553, 0.0808) (0.0003, 0.0032)	
EPICA Dome C	Estimated γ_1 Estimated γ_2	0.0668 0.0009	0.0833 0.0030	0.0973 0.0028
	Estimated se γ_1 Estimated se γ_2	0.0098 0.0009	0.0039 0.0004	0.0321 0.0033
	95% CI γ_1 95% CI γ_2	(0.0442, 0.0839) (-0.0014, 0.0024)	(0.0745, 0.0893) (0.0021, 0.0037)	(0.0065, 0.1329) (-0.0067, 0.0066)

The quadratic term for the middle period is found to be positive and significant at the 5% level at all locations.

Figure S.1 shows a reproduction of Figure 3 of the main paper on the left panels and the corresponding plots obtained by fitting model (S.1) on the right panels. Figure S.2 shows the scatterplots of these two quantities against one another.

Dome Fuji

Model (1) – Linear effect of temperature

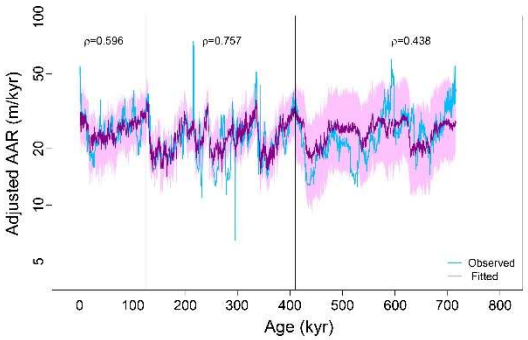

Model (S.1) – Quadratic effect of temperature

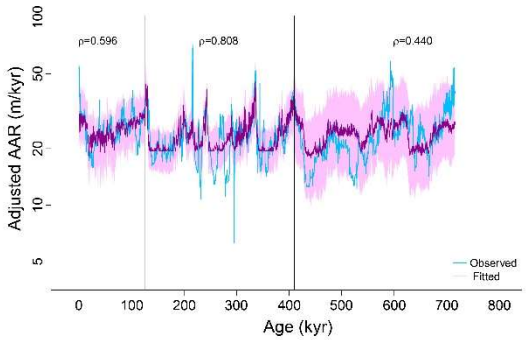

Lake Vostok

Model (1) – Linear effect of temperature

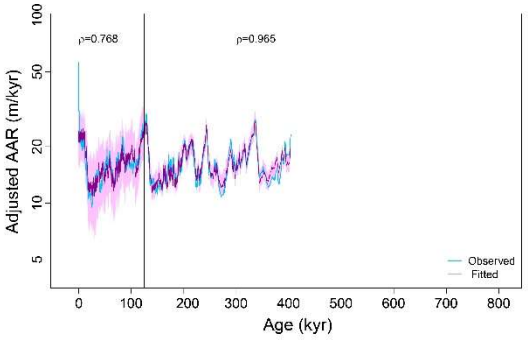

Model (S.1) – Quadratic effect of temperature

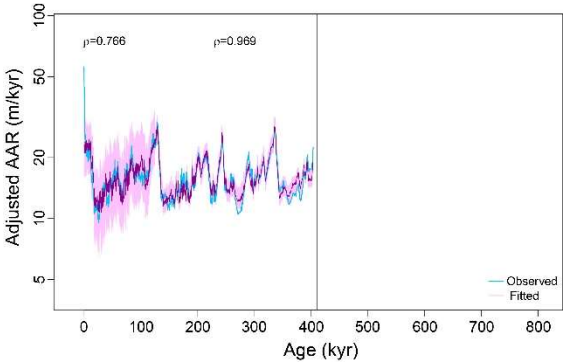

EPICA Dome C

Model (1) – Linear effect of temperature

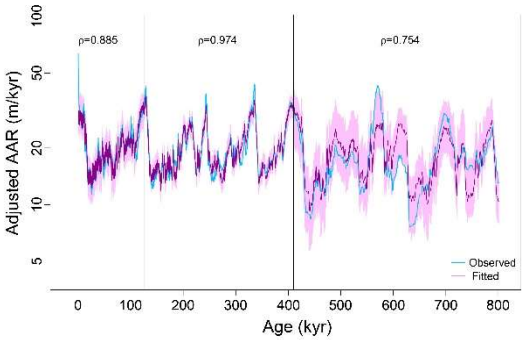

Model (S.1) – Quadratic effect of temperature

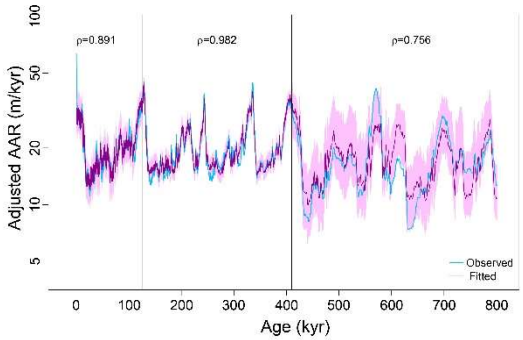

Figure S.1: The plots show the graphs of observed AAR adjusted for apparent thinning (blue line) and fitted AAR from model (1) (left) and (S.1) (right) adjusted for apparent thinning (purple line), in log scale labeled along vertical axis, versus age labeled along the horizontal axis. The pink shaded regions represent 95% coverage bootstrap confidence intervals for the purple curve. The two vertical black lines correspond to ages 125 kyr and 410 kyr. The sample correlation (ρ) between the observed and the fitted AAR is shown in each panel.

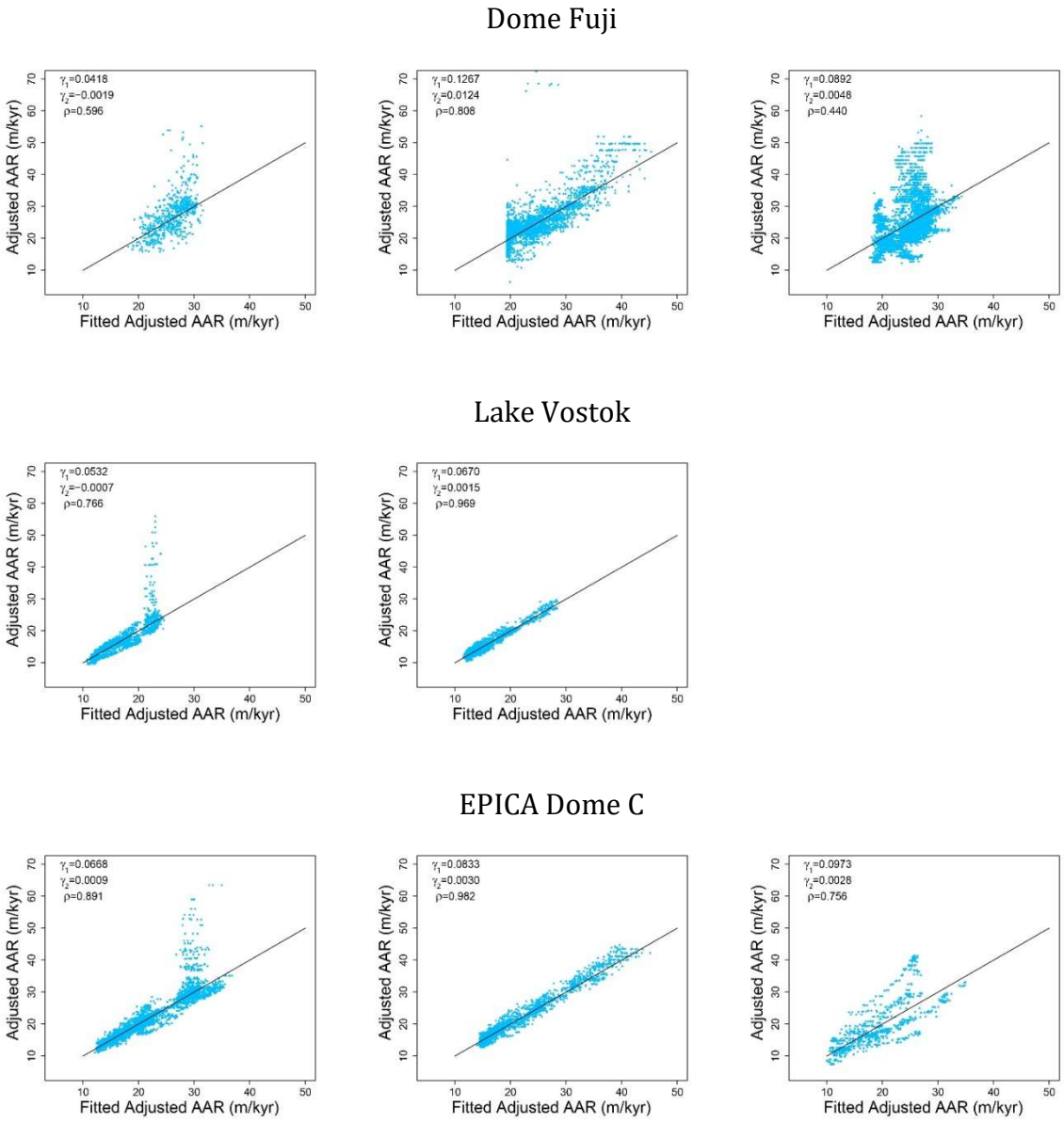

Figure S.2: The plots show scatters of the observed vs. fitted AAR adjusted for apparent thinning as per model (S.1), labeled along the vertical axis. The three plots in each row corresponds to the periods 0 to 125 kyr, 125 to 410 kyr and 410 to 800 kyr. The sample correlation (ρ) between the observed and the fitted AAR, along with the estimated parameters γ_1 and γ_2 are shown in each panel. The diagonal line in each plot indicates perfect fit.

It is seen that while the nonlinerity of the scatter in the middle period is removed once the quadratic term is introduced. However, the improvement in the correlation is only marginal. The instances of unusually large deviations from the fit at higher temperatures, particularly on the positive side remain as they did for the simpler model. The uncertainties captured by the standard errors and confidence intervals also remain at the earlier level. For the plot of Dome Fuji during the period 125 to 410 kyr, the concentration of points at the left end of the horizontal scale is a consequence of the small slope of the fitted quadratic function in the corresponding range of temperature.

The time plot of the observed AAR without any adjustment and its fitted versions from model (1) of the main paper and model (S.1) are shown side by side in Figure S.3.

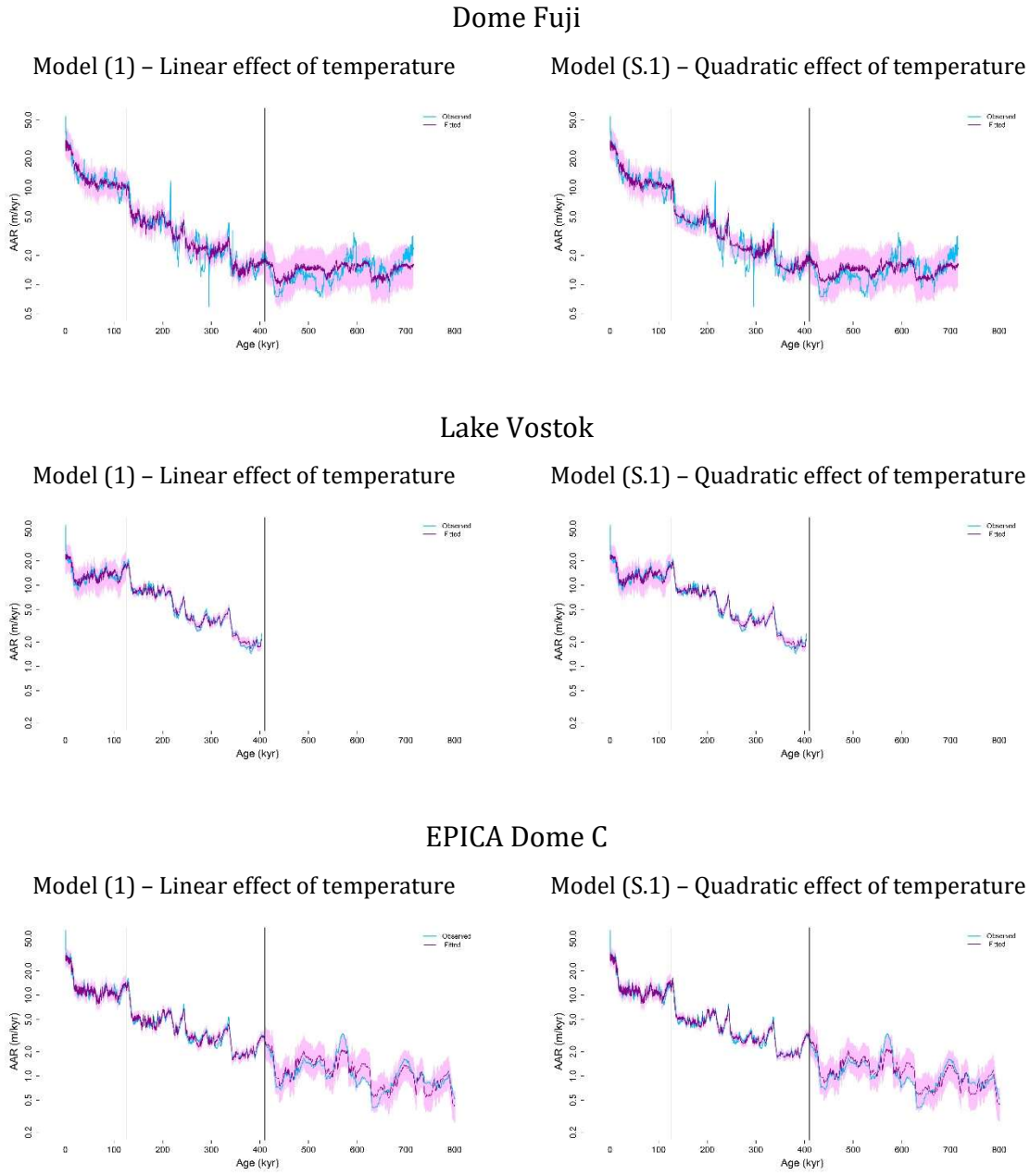

Figure S.3: The plots show the graphs of observed AAR adjusted for apparent thinning (blue line) and fitted AAR from model (1) (left) and (S.1) (right) adjusted for apparent thinning (purple line), in log scale labeled along vertical axis, versus age labeled along the horizontal axis. The pink shaded regions represent 95% coverage bootstrap confidence intervals for the purple curve. The two vertical black lines correspond to ages 125 kyr and 410 kyr. The sample correlation (ρ) between the observed and the fitted AAR is shown in each panel.

It is seen that the fits from the models with linear and quadratic effects of temperature produce comparable fits. Further, the bootstrap confidence intervals of the observed AAR are reasonably narrow except in the oldest period (possibly due to greater impact of measurement errors and unaccounted factors such as substrata effect at extreme depths). However, for any given location and time period, the intervals of AAR are narrower than those for the AAR adjusted for thinning/compression, shown in Figure S.1. Note the adjusted AAR is a version of the accumulation rate

(see the penultimate paragraph of Section 2 of the main paper.) This fact vindicates the authors' strategy of choosing AAR over accumulation rate for studying the effect of temperature.

2. A parametric model for the thinning function

The plots of the Apparent Accumulation Rate (AAR) given in Figure 2 of the main paper reveal a consistent pattern of gradual reduction. Faster thinning in the recent past, due to a greater scope of compaction, is generally followed by a period of slower thinning. Interestingly, the AAR in log scale exhibits a linearly decreasing pattern for the age of ice in the age range 125 to 410 kyr for all the three sites chosen over the region of Antarctica. This linear decline in the log scale is indicative of an exponentially decaying pattern of thinning. Further, for Dome Fuji and EPICA Dome C, where longer records are available, the general level of AAR eventually saturates to a minimum value. This pattern is captured by the following parametric version of the AAR model.

$$b_i \;=\; (1 \;+\gamma x_i)\left(b_0 e^{-\frac{z_i}{z_e}} \;+\; b_\infty\right)\xi_i \quad \text{for } 125 < z_i < 800 \tag{S.2}$$

Here, the factor $\left(b_0 e^{-\frac{z_i}{z_e}} \;+\; b_\infty\right)$ is a parametric form of $g(z_i)$ in model (1) of the main paper. The parameters $b_0 + b_\infty$ and b_∞ are the initial and the saturated values of AAR when the temperature deviation is zero. The parameter z_e is a time constant that controls the rate of reduction of AAR. Specifically, it is the time needed by the excess of AAR over b_∞ to reduce by a factor of e.

The parameter $b_\infty/(b_0 + b_\infty)$ represents the ratio of the long-run AAR with the AAR at the present time, as explained by the parametric model. We refer to this ratio as the long-term thinning factor.

2.1 Method of estimation

The fitting of this model is done by using the method of nonlinear least squares for the log-transformed AAR. The nonlinear least squares estimator $(\hat{\gamma},\ \hat{b}_0,\ \hat{z}_e, \hat{b}_\infty)'$ minimizes the sum of squared errors ,

$$\sum_{i:125<z_i<800} \left(\log(b_i) - \log(1+\gamma x_i) - \log\left(b_0 e^{-\frac{z_i}{z_e}} \;+\; b_\infty\right)\right)^2 .$$

Under the conditions of Theorem 3.2 of White and Domowitz 1984 and the additional assumption that $\log(\xi_i)$ is an autoregressive process of order 1 (as in Srivastava and Sengupta 2023), a consistent estimator of the covariance matrix of the estimator $(\hat{\gamma}, \hat{b}_0,\ \hat{z}_e, \hat{b}_\infty)'$ is given by

$$\hat{V} = \frac{1}{n}\left(\hat{F}'\hat{F}/n\right)^{-1}\left(\hat{F}'\,\hat{\Sigma}\,\hat{F}/n\right)\left(\hat{F}'\hat{F}/n\right)^{-1},$$

where n is the sample size, $\hat{F}$ is a $n \times 4$ matrix with i^{th} row

$$\left[\frac{x_i}{(1+\hat{\gamma}x_i)} \quad \frac{e^{-z_i/\hat{z}_e}}{\hat{b}_0 e^{-z_i/\hat{z}_e}+\hat{b}_\infty} \quad \frac{-\hat{b}_0\, z_i e^{-z_i/\hat{z}_e}}{\hat{z}_e{}^2\left(\hat{b}_0 e^{-z_i/\hat{z}_e}+\hat{b}_\infty\right)} \quad \frac{1}{\hat{b}_0 e^{-z_i/\hat{z}_e}+\hat{b}_\infty}\right],$$

and $\hat{\Sigma}$ is the $n \times n$ Toeplitz matrix with $(i,j)^{\text{th}}$ element $\hat{s}_{ij} = \frac{\hat{\sigma}^2}{1-\hat{\phi}^2}\,\hat{\phi}^{|i-j|}$

with $\hat{\phi} = \frac{\sum_{i=2}^n \hat{\varepsilon}_i\hat{\varepsilon}_{i-1}}{\sum_{i=2}^n \hat{\varepsilon}_i{}^2}$, $\hat{\sigma}^2 = \frac{1}{n}\sum_{i=2}^n\left(\hat{\varepsilon}_i - \hat{\phi}\,\hat{\varepsilon}_{i-1}\right)^2$, and

$$\hat{\varepsilon}_i = \log(b_i) - \log(1+\hat{\gamma}x_i) - \log\left(\hat{b}_0 e^{-\frac{z_i}{\hat{z}_e}} \;+\; \hat{b}_\infty\right) \text{ for } i = 1,2,\ldots,n.$$

The standard error of $b_\infty/(b_\infty + b_0)$, obtained by using the Delta method, is given by

$$\frac{1}{\left(\hat{b}_\infty+\hat{b}_0\right)^2}\ \sqrt{\hat{b}_0^2\ v_{4,4} \;+\hat{b}_\infty^2\ v_{2,2} \;-2\hat{b}_0\hat{b}_\infty\ v_{2,4}}\ ,$$

where $v_{i,j}$ is the $(i,j)^{\text{th}}$ element of matrix $\hat{V}$ for $i, j = 1,2,3,4$.

2.2 Results

Figure S.3 shows the plots of the observed AAR, adjusted for variation in temperature (obtained by dividing AAR with estimated value of $1 + \gamma x$), along with fitted value AAR, also adjusted for variation in temperature (obtained as the estimate of $b_0 e^{-\frac{z_i}{z_e}} + b_\infty$), versus age z in solid blue and orange lines, respectively. The adjusted AAR shown along the vertical axis is in the log scale. The fit looks adequate.

Table S.2: Parameter estimates of AAR model (1) along with estimated standard error

Location	γ (S.E.) (per ^{o}C)	z_e (S.E.) (kilo years)	b_0 (S.E.) (mm/year)	b_∞ (S.E.) (mm/year)	$b_\infty/(b_\infty + b_0)$ (S.E.)
Dome Fuji	0.0687	72.470	49.917	1.658	0.0322
	(0.0065)	(6.684)	(14.260)	(0.055)	(0.0085)
Lake Vostok	0.0508	126.266	46.203	0.547	0.0117
	(0.0052)	(26.694)	(9.639)	(1.180)	(0.0230)
EPICA Dome C	0.0626	138.635	26.540	1.342	0.0481
	(0.0036)	(14.547)	(4.075)	(0.170)	(0.0059)

Table S.2 shows the least squares estimates of parameters of model (S.2), along with the estimates of the long-term apparent thinning factor $b_\infty/(b_0 + b_\infty)$. The associated standard errors are shown below each estimate in parentheses.

Estimates of the parameters b_∞ and $b_\infty/(b_0 + b_\infty)$ for Lake Vostok are small with large standard errors. This is not surprising, as the data record at Lake Vostok covers a much shorter time period. Saturation of the thinning process is not prominent in the deepest layers of the ice sheet at Lake Vostok, due to the presence of water in the subglacial lake below the drilling site. Observed patterns of differential melting and freezing at the base of the ice sheet (Siegert et al. 2000) and flow of ice in the subglacial lake (Leonard et al. 2004) indicate significant quantities of water/heat exchange.

Apart from this anomaly at Lake Vostok, the estimated parameters at the three sites follow a similar pattern. The estimates of γ are consistent with the range of values obtained from the semiparametric AAR model fitted for smaller segments of age.

The initial rate of decline in AAR, plotted in the log scale in Figure S.4, is very much linear at all the three locations, before saturation is approached at Dome Fuji and EPICA Dome C. The smaller value of the time constant z_e at Dome Fuji is indicative of faster thinning, possibly due to lateral transport away from the site over the ages owing to its higher elevation. The smaller value of the long-term thinning factor may also have a similar explanation.

The estimates of the initial AAR $b_0 + b_\infty$ at Dome Fuji and Lake Vostok are somewhat higher than the contemporary precipitation records. This deviation is explained by the fact that the parameter is extrapolated from data records older than 125 kyr. AAR is the combined effect of precipitation, lateral flow and other prevailing factors during this period.

Dome Fuji

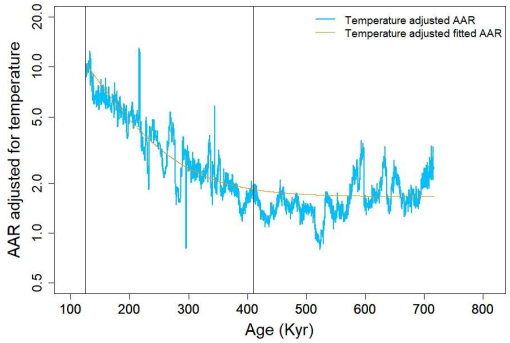

Lake Vostok

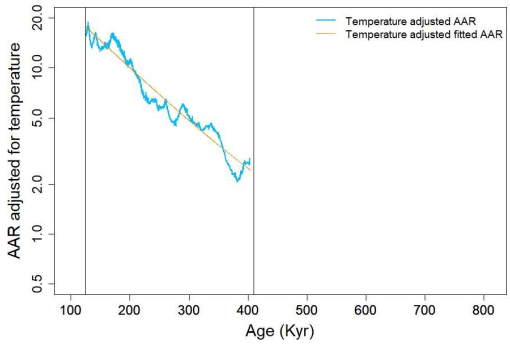

EPICA Dome C

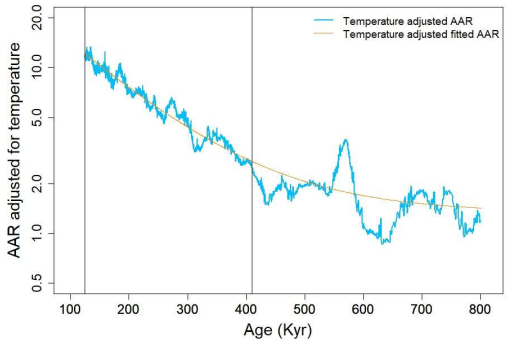

Figure S.4: The graphs of observed AAR adjusted for temperature (in blue line) and fitted AAR adjusted for temperature (in orange line) in log scale labeled along the vertical axis, versus age labeled along the horizontal axis for the ice age in the range 125 kyr to 800 kyr.

3. References

Leonard, K. et al. (2004). "Anomalous accumulation rates in the Vostok ice-core resulting from ice flow over Lake Vostok". In: *Geophysical Research Letters* 31.24, p. L24401.

Siegert, M. J. et al. (2000). "Water exchange between the subglacial Lake Vostok and the overlying ice sheet". In: *Nature* 403.6770, pp. 643–646.

Srivastava, R. and D. Sengupta (2023). *A semi-parametric model for ice accumulation rate and temperature based on Antarctic ice core data*. Preprint at http://arxiv.org/abs/2309.03782.

White, H. and I. Domowitz (1984). "Nonlinear regression with dependent observations". In: *Econometrica* 52.1, pp. 143–162.